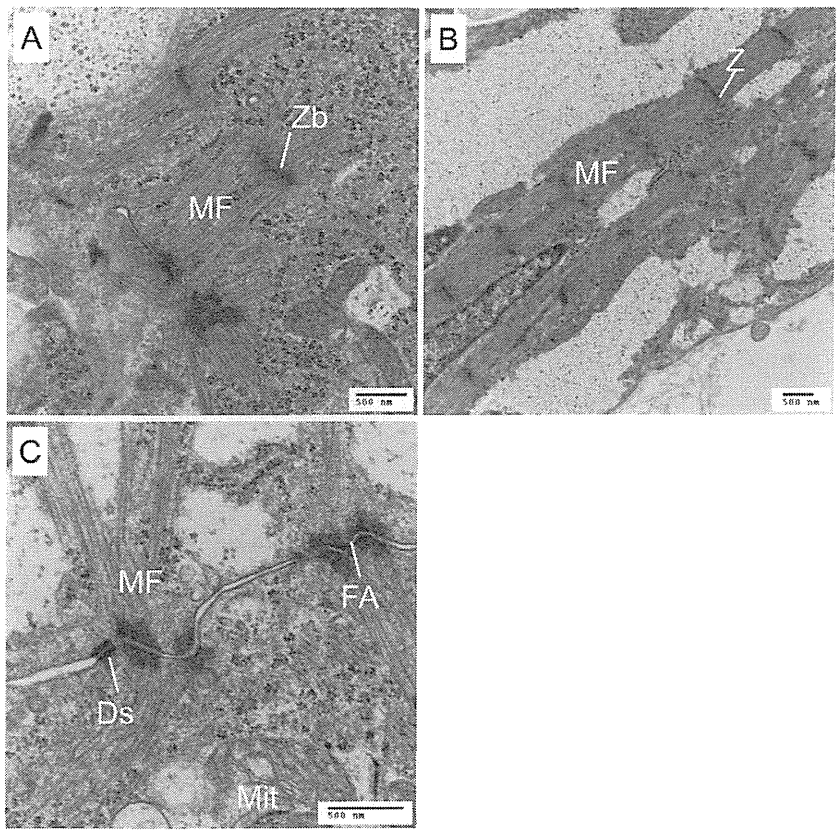

Figure 3. Transmission electron microscopy images of human-induced pluripotent stem cell-derived cardiomyocytes (hiPSC-CMs) at 14 days after cardiac differentiation. (**A**) hiPSC-CMs at 14 days contained myofibrils (MF) that lacked alignment or organized sarcomeric pattern. Scattered condensed Z-bodies (Zb) were also confirmed. (**B**) In some areas, a more developed pattern was noted in which myofibrils (MF) were held between a few of the Z-bands (Z). (**C**) CMs connected by desmosomes (Ds) and fascia adherens (FA) even at this early stage. Mitochondria (Mit) can be seen.

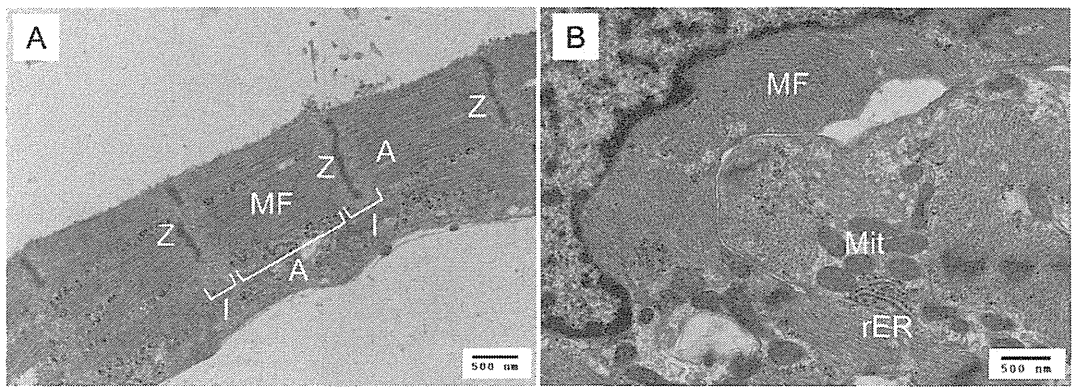

Figure 4. Transmission electron microscopy images of human-induced pluripotent stem cell-derived cardiomyocytes (hiPSC-CMs) at 30 days after cardiac differentiation. (**A**) hiPSC-CMs at 30 days appeared to be packed between parallel Z-bands. Some myofibrils (MF) showed A- (A) and I-bands (I). (**B**) Transverse section of sarcomere and rough endoplasmic reticulum (rER). Mitochondria (Mit) can be seen.

MLC2a-positive, and 56% were MLC2v/MLC2a double-positive CMs at 30-day differentiation. By day 360, MLC2v-positive/MLC2a-negative CMs increased to 60%, whereas MLC2v/MLC2a double-positive immature ventricular CMs decreased to 36% (**Figure 2F**).

Ultrastructural Analysis of hiPSC-CMs at 14-, 30-, 60-, 90-, 180-, and 360-Day Differentiation

hiPSC-CMs at 14-day differentiation contained myofibrils that lacked alignment or organized sarcomeric pattern, and were distributed diffusely in the cytoplasm in a disorganized fashion. Scattered patterns of condensed Z-bodies were also confirmed. However, in some areas, a more developed pattern was

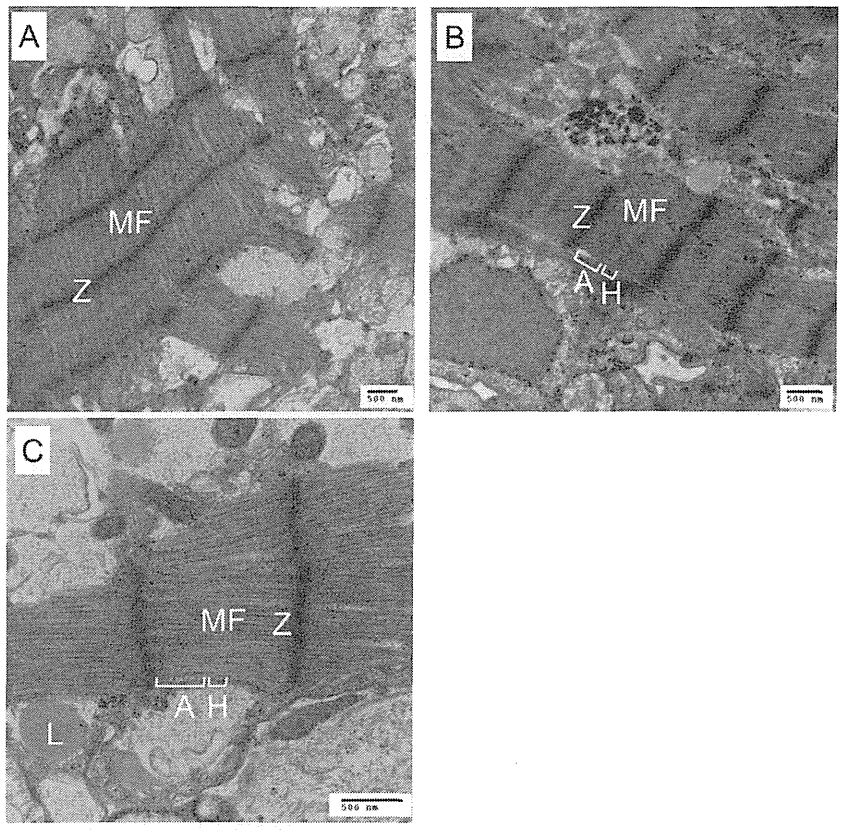

Figure 5. Transmission electron microscopy images of human-induced pluripotent stem cell-derived cardiomyocytes (hiPSC-CMs) at 60 (**A**), 90 (**B**), and 180 days (**C**) after cardiac differentiation. Between 60- and 180-day differentiation, ultrastructural maturation continued and formation of H-bands (H) can be seen. However, even at 180-day differentiation, M-bands are not apparent. Lipid droplets (L) can be seen in (**C**).

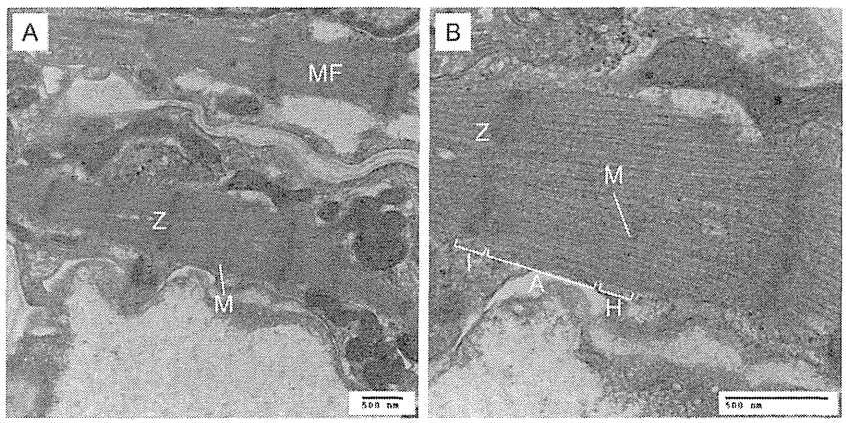

Figure 6. Transmission electron microscopy images of human-induced pluripotent stem cell-derived cardiomyocytes (hiPSC-CMs) at 360 days after cardiac differentiation. (**A**,**B**) In addition to discrete A-, H-, I-, and Z-bands, M-bands (M) are also noted in a minority of the cells within the sarcomeres.

noted in which myofibrils were held between a few of the Z-bands (**Figure 3**). However, A-, H-, I-, and M-bands were not recognized. CMs were connected by desmosomes and fascia adherens at this early stage.

At 30-day differentiation, nascent myofibrils decreased and appeared to be packed between Z-bands. Parallel Z-bands were demonstrated to confine the myofibrils in the typical sarcomeric pattern. Some myofibrils showed A- and I-bands. However, they still lacked the formation of H-, and M-bands (**Figure 4**). Mitochondria and rough endoplasmic reticulum were also noted, as previously reported.[13]

Between 60- and 90-day differentiation, ultrastructural maturation continued and formation of H-bands could be observed. However, even at 180-day differentiation, M-bands could not be detected (**Figure 5**).

Finally, at 360-day differentiation, in addition to discrete A-, H-, I-, and Z-bands, M-bands were first noted in a minority of the cells within the sarcomeres (**Figure 6**). Myofibrils appeared to be tightly packed and distributed in an oriented fashion. The amount of sarcomeric structure in a single CM continued to increase, but was still scarce compared with an adult CM. Even at this stage, different degrees of organization

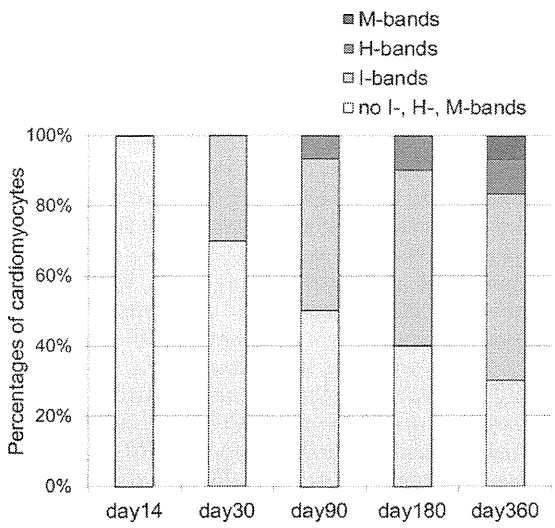

Figure 7. Percentages of the cardiomyocytes (CMs) having I-, H-, and M-bands at 14, 30, 90, 180, 360 days after cardiac differentiation. The amount of CMs with I- and H-bands increased through the long-term culture and M-bands were first noted in 360-day CMs.

existed simultaneously in the same EB.

We evaluated 30 CMs with sarcomeres on randomly selected electron micrographs to assess the maturation process of sarcomeres quantitatively. Figure 7 shows the percentages of CMs having I-, H-, and M-bands at 14-, 30-, 90-, 180-, 360-day differentiation.

Expression of Cardiac-Specific Genes

Leucine-rich repeat-containing protein 39 (*LRRC39*), myomesin 1 (*MYOM1*), and 2 (*MYOM2*), components of M-bands,[18] increased at 360-day differentiation compared with 30-day differentiation, supporting the observation of M-band formation in 360-day hiPSC-CMs (Figure 8). However, the expression levels of the M-band-specific proteins in the hiPSC-CMs were lower compared with those of the adult heart. The expression of cardiac troponin-T (*cTnT*), myosin heavy chain 6 (*MYH6*), myosin heavy chain 7 (*MYH7*), and myosin regulatory light chain 2 (*MYL2*) also increased after the 1-year culture. However, the expression levels of cardiac-specific genes in the hiPSC-CMs were also considerably lower than those in the adult heart left ventricle or left atrium, and in the fetal heart. The expression levels of gap junction α-1 protein were significantly decreased in 180-day and 360-day hiPSC-CMs compared with 30-day hiPSC-CMs.

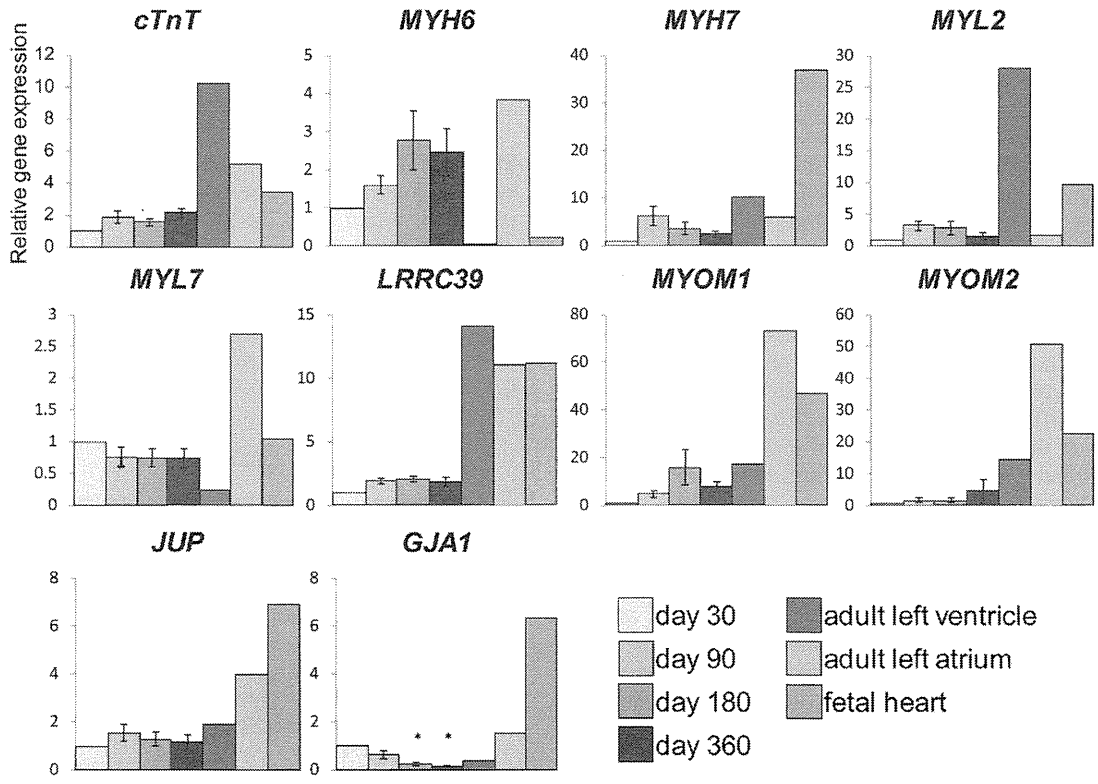

Figure 8. Real-time quantitative polymerase chain reaction analyses for *cTnT*, *MYH6*, *MYH7*, *MYL2*, *MYL7*, *LRRC39*, *MYOM1*, *MYOM2*, *JUP*, and *GJA1* expression in beating embryoid bodies (EB) from human-induced pluripotent stem cell-derived cardiomyocytes (hiPSC-CMs) at 30, 90, 180, and 360 days, in the adult left ventricle, adult left atrium, and fetal heart. The changes in gene expression levels were compared with those of hiPSC-CMs at 30-day differentiation. *cTnT*, cardiac troponin-T; *MYH6*, myosin heavy chain 6; *MYH7*, myosin heavy chain 7; *MYL2*, myosin regulatory light chain 2; *MYL7*, myosin regulatory light chain 7; *LRRC39*, leucine-rich repeat-containing protein 39; *MYOM1*, myomesin 1; *MYOM2*, myomesin 2; *JUP*, junction plakoglobin; *GJA1*, gap junction α-1 protein. *P<0.05 vs. 30-days EBs.

Discussion

In this study, we demonstrated that hiPSC-CMs continue to mature through a 1-year culture. This is the first report of the feasibility of 1-year 2D culture of hiPSC-CMs and description of the sarcomeric maturation process represented by the emergence of M-bands and the increase in the cardiac-specific gene expressions.

So far, the reported ultrastructure of hiPSC-CMs has been immature and their maturation process remained unknown.[4,13,14] Human embryonic stem cell-derived cardiomyocytes (hESC-CMs) are reported to follow a roughly similar maturation process to that reported both in vivo and in an in-vitro murine ES model.[19–24] The hiPSC-CMs in the present study showed a similar maturation process to that of hESC-CMs.[25] At first, narrow, diffusely distributed, and frequently not well aligned myofibrils, resembling those of hiPSC-CMs at 14 days, developed into sarcomeres with clear band patterns including the Z-, I-, and A-bands, responding to hiPSC-CMs at between 30 and 90 days, and ultimately resulted in the generation of well-designed sarcomeres with A-, H-, I-, and M-bands. The ultrastructural findings of hiPSC-CMs in the literature now available relate to around 30 days of differentiation, and only Z- and I-bands have been visible.[4,13,14] In our study, the 30-day hiPSC-CMs similarly showed only Z- and I-bands, not H- or M-bands. Notably, we are the first to find that only 360-day hiPSC-CMs, not 180-day hiPSC-CMs, show a mature sarcomeric structure with M-bands. However, even at 360-day differentiation, different degrees of organization patterns existed simultaneously in the same EB and homogeneous maturation was not confirmed. Our 1-year culture system was able to confirm more mature sarcomeric structures than previously reported, but still not that of adult CMs. It is reported that human CMs derived from fetal hearts do not achieve full ultrastructural maturity and that myofibrillar development continues throughout the entire fetal period.[22] The insufficient maturation of hiPSC-CMs after long-term culture could be explained by several factors. In vitro culturing conditions lack the presence of adjacent non-myocyte proliferating cells, which play an important role in the maturation of CMs via paracrine and humoral signals in vivo. In addition, the CMs grown in the absence of hemodynamic workload typical of in vivo working CMs are reported to lack appropriate ultrastructural development.[26] The differences between in vitro and in vivo conditions, such as the absence of humoral factors and organized mechanical and electrical stress in vitro, might result in delayed ultrastructural maturation.

In electron micrographs of the sarcomere, the M-band appears as a series of parallel electron-dense lines in the central zone of the A-band. The M-band has been reported to play a role not only in mechanical stability in the activated sarcomere, such as reducing the intrinsic instability of thick filaments and helping titin to maintain order in sarcomeres, but also in the biomechanical conditions in contracting muscle such as stress sensing.[27] M-band formation was confirmed in the latest stage and has been considered the endpoint of myofibrillar maturation.[18,21] The lower expression levels of the M-band-specific proteins in the hiPSC-CMs compared with the adult heart might be associated with the delayed appearance of M-bands. Maturation of iPSC-CMs is critical for their application in regenerative medicine, as well as for investigating the mechanisms underlying inherited cardiac diseases. Techniques to promote the maturation of ESC-CMs, such as 3D culture methodology,[28] electric stimulation,[29] and coculture with non-cardiomyocytes[30] may be applicable to iPSC-CMs to overcome the problem, although it has not been fully investigated in hiPSC-CMs. Improved methods are needed to produce homogeneous, mature iPSC-CMs.

In addition to ultrastructural maturation, there was a significant increase in the size of hiPSC-CMs after long-term culture, supporting the process of morphological maturation. Also, the lower rate of beating of 360-day hiPSC-CMs compared with 30-day hiPSC-CMs suggested electrophysiological maturation, because it has been reported that the resting membrane potential becomes progressively more negative in the developing atrial and ventricular myocytes, which correlates with an increasing presence of I_{K1}, and ultimately, the fetal atrial and ventricular myocytes exhibit stable resting membrane potentials with little automaticity.[31]

Changes in the expression patterns of MLC2v and MLC2a occur during the maturation process.[32] hiPSC-CMs were thought to be immature and similar to human fetal CMs because of the presence of a number of MLC2v/MLC2a double-positive CMs.[33] Our immunostaining analysis demonstrated that the percentage of MLC2v/MLC2a double-positive hiPSC-CMs decreased after long-term culture, accompanied by an increase in MLC2v-positive/MLC2a-negative hiPSC-CMs, suggesting maturing of the ventricular-type CMs.

This study also showed for the first time, changes in the expression levels of cardiac-specific genes and genes related to intercalated discs throughout the 1-year culture. The cardiac-specific genes tended to increase during 1-year culture, supporting the maturation process of hiPSC-CMs. The connexin (gap junction proteins) are reported to be more abundant in the neonate than the adult.[34] The significant decrease in *GJA1* expression levels in 180- and 360-day hiPSC-CMs compared with 30-day hiPSC-CMs also suggested maturation of hiPSC-CMs.

Study Limitations

We used microdissected beating EBs for the gene expression studies. The fact that EBs contain CMs at various stages of differentiation, as well as non-CMs, might obscure the results of the gene expression studies. We conducted immunostaining analysis of single cells from microdissected beating EBs 3 days after enzymatic dispersion, which might allow non-CMs to increase and affect the results of the percentage of CMs in the beating EBs.

Conclusions

The current study demonstrated developmental changes in the ultrastructural, immunocytological, and gene expression properties of hiPSC-CMs. Our results confirmed mature sarcomeric structure with M-band formation in long-term culture of hiPSC-CMs for the first time, which provides a new insight into the maturation process of hiPSC-CMs. For application of homogeneous mature hiPSC-CMs in regenerative medicine and in vitro modeling of human cardiac diseases, further maturation of cardiac cells will be needed.

Acknowledgments

We thank Aya Umehara, Masako Tanaka, Kyoko Yoshida, and the Division of Electron Microscopic Study, Center for Anatomical Studies, Kyoto University Graduate School of Medicine for technical assistance.

Sources of Funding

This work was supported by research grants from the Ministry of Education, Culture, Science, and Technology of Japan (T.M. and M.H.), Suzuken Memorial Foundation (T. Kimura), Fujiwara Memorial Foundation

(T.M.), the Uehara Memorial Foundation (M.H.), and health science research grants from the Ministry of Health, Labor and Welfare of Japan for Clinical Research on Measures for Intractable Diseases (T.M. and M.H.).

Disclosures

None.

References

1. Takahashi K, Tanabe K, Ohnuki M, Narita M, Ichisaka T, Tomoda K, et al. Induction of pluripotent stem cells from adult human fibroblasts by defined factors. *Cell* 2007; **131:** 861–872.
2. Zhang J, Wilson GF, Soerens AG, Koonce CH, Yu J, Palecek SP, et al. Functional cardiomyocytes derived from human-induced pluripotent stem cells. *Circ Res* 2009; **104:** e30–e41.
3. Moretti A, Bellin M, Welling A, Jung CB, Lam JT, Bott-Flügel L, et al. Patient-specific induced pluripotent stem-cell models for long-QT syndrome. *N Engl J Med* 2010; **363:** 1397–1409.
4. Novak A, Barad L, Zeevi-Levin N, Shick R, Shtrichman R, Lorber A, et al. Cardiomyocytes generated from CPVT^{D307H} patients are arrhythmogenic in response to β-adrenergic stimulation. *J Cell Mol Med* 2012; **16:** 468–482.
5. Choi SH, Jung SY, Kwon SM, Baek SH. Perspectives on stem cell therapy for cardiac regeneration. *Circ J* 2012; **76:** 1307–1312.
6. Zwi L, Caspi O, Arbel G, Huber I, Gepstein A, Park IH, et al. Cardiomyocyte differentiation of human-induced pluripotent stem cells. *Circulation* 2009; **120:** 1513–1523.
7. Germanguz I, Sedan O, Zeevi-Levin N, Shtrichman R, Barak E, Ziskind A, et al. Molecular characterization and functional properties of cardiomyocytes derived from human inducible pluripotent stem cells. *J Cell Mol Med* 2011; **14:** 38–51.
8. Ma J, Guo L, Fiene SJ, Anson BD, Thomson JA, Kamp TJ, et al. High purity human-induced pluripotent stem cell-derived cardiomyocytes electrophysiological properties of action potentials and ionic currents. *Am J Physiol Heart Circ Physiol* 2011; **301:** H2006–H2017.
9. Tanaka T, Tohyama S, Murata M, Nomura F, Kaneko T, Chen H, et al. In vitro pharmacologic testing using human-induced pluripotent stem cell-derived cardiomyocytes. *Biochem Biophys Res Commun* 2009; **385:** 497–502.
10. Xi J, Khalil M, Shishechian N, Hannes T, Pfannkuche K, Liang H, et al. Comparison of contractile behavior of native murine ventricular tissue and cardiomyocytes derived from embryonic or induced pluripotent stem cells. *FASEB J* 2010; **24:** 2739–2751.
11. Kuzmenkin A, Liang H, Xu G, Pfannkuche K, Eichhorn H, Fatima A, et al. Functional characterization of cardiomyocytes derived from murine induced pluripotent stem cells in vitro. *FASEB J* 2009; **23:** 4168–4180.
12. Jonsson MK, Vos MA, Mirams GR, Duker G, Sartipy P, de Boer TP, et al. Application of human stem cell-derived cardiomyocytes in safety pharmacology requires caution beyond hERG. *J Mol Cell Cardiol* 2012; **52:** 998–1008.
13. Gherghiceanu M, Barad L, Novak A, Reiter I, Itskovitz-Eldor J, Binah O, et al. Cardiomyocytes derived from human embryonic and induced pluripotent stem cells: Comparative ultrastructure. *J Cell Mol Med* 2011; **15:** 2539–2551.
14. Fujiwara M, Yan P, Otsuji TG, Narazaki G, Uosaki H, Fukushima H, et al. Induction and enhancement of cardiac cell differentiation from mouse and human-induced pluripotent stem cells with cyclosporine-A. *PLoS One* 2011; **6:** e16734.
15. Yoshida Y, Takahashi K, Okita K, Ichisaka T, Yamanaka S. Hypoxia enhances the generation of induced pluripotent stem cells. *Cell Stem Cell* 2009; **5:** 237–241.
16. Dubois NC, Craft AM, Sharma P, Elliott DA, Stanley EG, Elefanty AG, et al. SIRPA is a specific cell-surface marker for isolating cardiomyocytes derived from human pluripotent stem cells. *Nat Biotechnol* 2011; **29:** 1011–1018.
17. Yang L, Soonpaa MH, Adler ED, Roepke TK, Kattman SJ, Kennedy M, et al. Human cardiovascular progenitor cells develop from a KDR$^+$ embryonic-stem-cell-derived population. *Nature* 2008; **453:** 524–528.
18. Will RD, Eden M, Just S, Hansen A, Eder A, Frank D, et al. Myomasp/LRRC39, a heart- and muscle-specific protein, is a novel component of the sarcomeric M-band and is involved in stretch sensing. *Circ Res* 2010; **107:** 1253–1264.
19. Beharvand H, Azarnia M, Parivar K, Ashtiani SK. The effect of extracellular matrix on embryonic stem cell-derived cardiomyocytes. *J Mol Cel Cardiol* 2005; **38:** 495–503.
20. Baharvand H, Piryaei A, Rohani R, Taei A, Heidari MH, Hosseini A. Ultrastructural comparison of developing mouse embryonic stem cell- and in vivo-derived cardiomyocytes. *Cell Biol Int* 2006; **30:** 800–807.
21. Anversa P, Olivetti G, Bracchi PG, Loud AV. Postnatal development of the M-band in rat cardiac myofibrils. *Circ Res* 1981; **48:** 561–568.
22. Kim HD, Kim DJ, Lee IJ, Rah BJ, Sawa Y, Schaper J. Human fetal heart development after mid-term: Morphometry and ultrastructural study. *J Mol Cell Cardiol* 1992; **24:** 949–965.
23. Legat MJ. Sarcomerogenesis in human myocardium. *J Mol Cell Cardiol* 1970; **1:** 425–437.
24. Yu L, Gao S, Nie L, Tang M, Huang W, Luo H, et al. Molecular and functional changes in voltage-gated Na^+ channels in cardiomyocytes during mouse embryogenesis. *Circ J* 2011; **75:** 2071–2079.
25. Snir M, Kehat I, Gepstein A, Coleman R, Itskovitz-Eldor J, Livne E, et al. Assessment of the ultrastructural and proliferative properties of human embryonic stem cell-derived cardiomyocytes. *Am J Physiol Heart Circ Physiol* 2003; **285:** H2355–H2363.
26. Bishop SP, Anderson PG, and Tucker DC. Morphological development of the rat heart growing in oculo in the absence of hemodynamic work load. *Circ Res* 1990; **66:** 84–102.
27. Agarkova I, Perriard JC. The M-band: An elastic web that crosslinks thick filaments in the center of the sarcomere. *Trends Cell Biol* 2005; **15:** 477–485.
28. Ou DB, He Y, Chen R, Teng JW, Wang HT, Zeng D, et al. Three-dimensional co-culture facilitates the differentiation of embryonic stem cells into mature cardiomyocytes. *J Cell Biochem* 2011; **112:** 3555–3562.
29. Chen MQ, Xie X, Wilson KD, Sun N, Wu JC, Giovangrandi L, et al. Current-controlled electrical point-source stimulation of embryonic stem cells. *Cell Mol Bioeng* 2009; **2:** 625–635.
30. Kim C, Majdi M, Xia P, Wei KA, Talantova M, Spiering S, et al. Non-cardiomyocytes influence the electrophysiological maturation of human embryonic stem cell-derived cardiomyocytes during differentiation. *Stem Cells Dev* 2010; **19:** 783–795.
31. He JQ, Ma Y, Lee Y, Thomson JA, Kamp TJ. Human embryonic stem cells develop into multiple types of cardiac myocytes: Action potential characterization. *Circ Res* 2003; **93:** 32–39.
32. Kubalak SW, Miller-Hance WC, O'Brien TX, Dyson E, Chien KR. Chamber specification of atrial myosin light chain-2 expression precedes septation during murine cardiogenesis. *J Biol Chem* 1994; **269:** 16961–16970.
33. Mummery CL, Zhang J, Ng ES, Elliott DA, Elefanty AG, Kamp TJ. Differentiation of human embryonic stem cells and induced pluripotent stem cells to cardiomyocytes: A methods overview. *Circ Res* 2012; **111:** 344–358.
34. Allah EA, Tellez JO, Yanni J, Nelson T, Monfredi O, Boyett MR, et al. Changes in the expression of ion channels, connexins and Ca^{2+}-handling proteins in the sino-atrial node during postnatal development. *Exp Physiol* 2011; **96:** 426–438.

Supplementary Files

Supplementary File 1

Table S1. Primer Sequences Used for Real-Time qPCR Analysis

Supplementary File 2

Movie S1. 360-day-old beating embryoid bodies.

Please find supplementary file(s);
http://dx.doi.org/10.1253/circj.CJ-12-0987

A novel mutation in the transmembrane nonpore region of the *KCNH2* gene causes severe clinical manifestations of long QT syndrome

Li Liu, MD,* Kenshi Hayashi, MD, PhD,† Tomoya Kaneda, MD, PhD,‡ Hidekazu Ino, MD, PhD,† Noboru Fujino, MD, PhD,† Katsuharu Uchiyama, MD, PhD,† Tetsuo Konno, MD, PhD,† Toyonobu Tsuda, MD,† Masa-aki Kawashiri, MD, PhD,† Kosei Ueda, MD, PhD,‡ Toshinori Higashikata, MD, PhD,‡ Wen Shuai, MS,§ Sabina Kupershmidt, PhD,§ Haruhiro Higashida, MD, PhD,* Masakazu Yamagishi, MD, PhD†

From the *Department of Biophysical Genetics, Kanazawa University Graduate School of Medical Science, Kanazawa, Japan, †Division of Cardiovascular Medicine, Kanazawa University Graduate School of Medical Science, Kanazawa, Japan, ‡Komatsu Municipal Hospital, Komatsu, Japan and §Anesthesiology Research Division, Vanderbilt University School of Medicine, Nashville, Tennessee.*

BACKGROUND Long QT syndrome (LQTS) is characterized by prolonged ventricular repolarization and variable clinical course with arrhythmia-related syncope and sudden death. Mutations in the nonpore region of the LQTS-associated *KCNH2* gene (also known as hERG) are mostly associated with coassembly or trafficking abnormalities, resulting in haplotype insufficiency and milder clinical phenotypes compared with mutations in the pore domain.

OBJECTIVE To investigate the effect of a nonpore mutation on the channel current, which was identified from an LQTS family with severe clinical phenotypes.

METHODS Two members of a Japanese family with LQTS were searched for mutations in *KCNQ1*, *KCNH2*, *SCN5A*, *KCNE1*, *KCNE2*, and *KCNJ2* genes by using automated DNA sequencing. We characterized the electrophysiological properties and glycosylation pattern of the mutant channels by using patch clamp recording and Western blot analysis.

RESULTS In the LQTS patient with torsades de pointes and cardiopulmonary arrest, we identified the novel T473P mutation in the transmembrane nonpore region of *KCNH2*. The proband's father carried the same mutation and showed prolonged corrected QT interval and frequent torsades de pointes in the presence of hypokalemia following the administration of garenoxacin. Patch clamp analysis in heterologous cells showed that hERG T473P channels generated no current and exhibited a dominant negative effect when coexpressed with wild-type protein. Only incompletely glycosylated hERG T473P channels were observed by using Western blot analysis, suggesting impaired trafficking.

CONCLUSIONS These results demonstrated that a trafficking-deficient mutation in the transmembrane nonpore region of *KCNH2* causes a dominant negative effect and a severe clinical course in affected patients.

KEYWORDS Long QT syndrome; *KCNH2*; Nonpore region; Trafficking deficient; Dominant negative

ABBREVIATIONS **ECG** = electrocardiogram; $\mathbf{I_{Kr}}$ = delayed rectifier K^+ current; **LQT2** = long QT syndrome type 2; **LQTS** = long QT syndrome; **QTc** = corrected QT; **TdP** = torsades de pointes

(Heart Rhythm 2013;10:61–67)

Introduction

Long QT syndrome (LQTS) is characterized by prolonged ventricular repolarization and malignant arrhythmia leading to syncope, cardiac arrest, and sudden death.[1] Genetic studies have so far identified 13 forms of congenital LQTS caused by mutations in genes of cardiac ion channels or ion channel modulators, including membrane adapters.[2] The acquired form of LQTS is more common than the congenital form; risk factors include drugs administered for noncardiac conditions, over-the-counter drugs, hypokalemia, bradycardia, and genetic variations in ion channel genes.[3]

The *KCNH2* gene encodes the Kv11.1 protein α subunit (hERG) that underlies the rapidly activating delayed rectifier K^+ current (I_{Kr}) in the heart, which is active during phases 2 and 3 of the cardiac action potential and plays an important role in cardiac repolarization. Mutations in *KCNH2* are responsible for LQTS type 2 (LQT2), and many mutations or polymorphisms in this gene have been identified in patients with both congenital and acquired LQTS.[4–7] Previous studies showed

The first 3 authors contributed equally to this work. This study was supported in part by grants from the Ministry of Health, Labour and Welfare of Japan. **Address reprint requests and correspondence:** Kenshi Hayashi, MD, PhD, Division of Cardiovascular Medicine, Kanazawa University Graduate School of Medical Science, 13-1, Takara-machi, Kanazawa, Ishikawa 920-8640, Japan. E-mail address: kenshi@med.kanazawa-u.ac.jp.

1547-5271/$-see front matter http://dx.doi.org/10.1016/j.hrthm.2012.09.053

that patients with mutations in the N-terminal, transmembrane nonpore, and C-terminal regions have a significantly decreased incidence of cardiac events than those with missense mutations in the pore region (S5-loop-S6), which appear to cause dominant negative effects.[8,9]

In the present study, we identified a novel missense mutation in the transmembrane nonpore region of the *KCNH2* gene that resulted in an amino acid substitution of threonine for proline acid at position 473 (T473P) in 2 members of a Japanese family with LQTS. The proband and his father showed significantly prolonged corrected QT (QTc) interval and torsades de pointes (TdP). The electrophysiological study showed that the T473P genetic change was a dominant negative mutation that led to loss of *KCNH2* function, and Western blot analysis indicated that this mutant had a trafficking defect.

Methods

DNA isolation and mutation analysis

Genomic DNA was isolated from the subjects' white blood cells by using conventional methods and was amplified by using standard polymerase chain reaction. All exons of the *KCNQ1*, *KCNH2*, *SCN5A*, *KCNE1*, *KCNE2*, and *KCNJ2* genes were sequenced by using an ABI PRISM 310 Genetic Analyzer.

Plasmid constructs and electrophysiology

The hERG cDNA was cloned into the mammalian expression vector pSI (Promega, Madison, WI). The T473P mutation was constructed by using an overlap extension strategy.

CHO-K1 cells were cultured and transiently transfected with wild-type (WT) hERG (1 μg) alone, hERG WT and hERG T473P (1 μg each), or hERG T473P (1 μg) alone by using FuGENE 6 Transfection Reagent. Cells were also cotransfected with an appropriate amount of the green fluorescent protein cloned into the pCGI vector for a total of 3 μg of cDNA per transfection. Cells displaying green fluorescence 48–72 hours after transfection were subjected to electrophysiological analysis. To test whether LQT2 mutations undergo pharmacological rescue, E4031 or thapsigargin (Alomone Labs, Jerusalem, Israel) was added to the culture media before the experimental study.

Membrane currents were studied essentially as described previously.[10] Data were acquired by using pCLAMP software (version 8.2; Axon Instruments/Molecular Devices, Sunnyvale, CA). Pooled data were expressed as mean ± standard error, and statistical comparisons were made (Origin 8.6, OriginLab, Northampton, MA) with $P < .05$ considered as significant.

Western blot analysis

Western blotting was performed as described previously.[11,12] Briefly, 2 days posttransfection, whole-cell lysates were prepared as described previously[11] by using a lysis buffer containing 50 mM Tris, 150 mM NaCl, 0.25% Triton X-100, 5 mM NaF, and protease inhibitors. Ten micrograms of cell extracts was loaded into a 7% polyacrylamide gel and prepared for polyacrylamide gel electrophoresis and Western Blot analysis. Following transfer onto nitrocellulose membranes, rabbit anti-hERG primary antibody (Alomone Labs; 1:400) and HRP-linked donkey anti-rabbit secondary antibody (Amersham Biosciences/GE Healthcare Life Sciences, Uppsala, Sweden; 1:10,000) were applied, and the bands were visualized with ECL (Amersham Biosciences/GE Healthcare Life Sciences).

Results

Clinical characterization and genetic analysis

The proband (Figure 1E, arrow) was a 37-year-old man who had syncope and was diagnosed with epilepsy at the age of 7. He had been treated with 150 mg of phenytoin; however, syncope still occurred several times a year. An electrocardiogram (ECG) taken during a routine health checkup at the age of 37 showed a mild prolongation of the QTc interval of 455 ms (Figure 1A, top). Early one morning, approximately 1 month after the health examination, the patient suddenly experienced cardiopulmonary arrest and was found to have ventricular fibrillation by the emergency crew. He received electrical defibrillation twice with an automated external defibrillator and was brought to the emergency department of our hospital. He had a significantly prolonged QTc interval of 566 ms upon admission (Figure 1A, middle). After admission, he experienced repeated TdP (Figure 1A, bottom). Temporary transvenous ventricular pacing was initiated to prevent pauses that may trigger TdP, and beta-blocker was also administered for symptomatic LQTS. He received an implantable cardioverter-defibrillator on his 21st day of hospitalization. Phenytoin was discontinued after hospital admission since his syncope was considered to be unrelated to epilepsy. He had not experienced syncope since the initiation of beta-blocker therapy.

The proband's father was also observed to have a prolongation of QTc interval at 526 ms during a family study for LQTS (Figure 1B, top) but did not have a history of syncope at that time. He had been treated with bisoprolol, valsartan, and amlodipine for hypertension since his early 60s. At the age of 74, he was afflicted with a respiratory tract infection and hypokalemia (2.9 mEq/L) as indicated by a blood test. He was prescribed 400 mg of garenoxacin once daily for the respiratory infection and subsequently developed syncope during the night. The ECG upon admission showed significant prolongation of QTc (668 ms) (Figure 1B, middle), and he experienced repeated TdP after admission (Figure 1B, bottom). He promptly discontinued the garenoxacin treatment, and instead received a replacement of potassium and temporary transvenous ventricular pacing. Bisoprolol was continued after this cardiac event. One morning, at the age of 75, he suffered a fatal cardiopulmonary arrest. Since hypokalemia (3.0 mEq/L) had been detected again during an outpatient visit a few days earlier, it is likely that TdP and ventricular fibrillation may have led to this fatal event.

Genetic analysis was performed after obtaining written informed consent, which revealed that both the proband and his father had a missense mutation consisting of an A to C

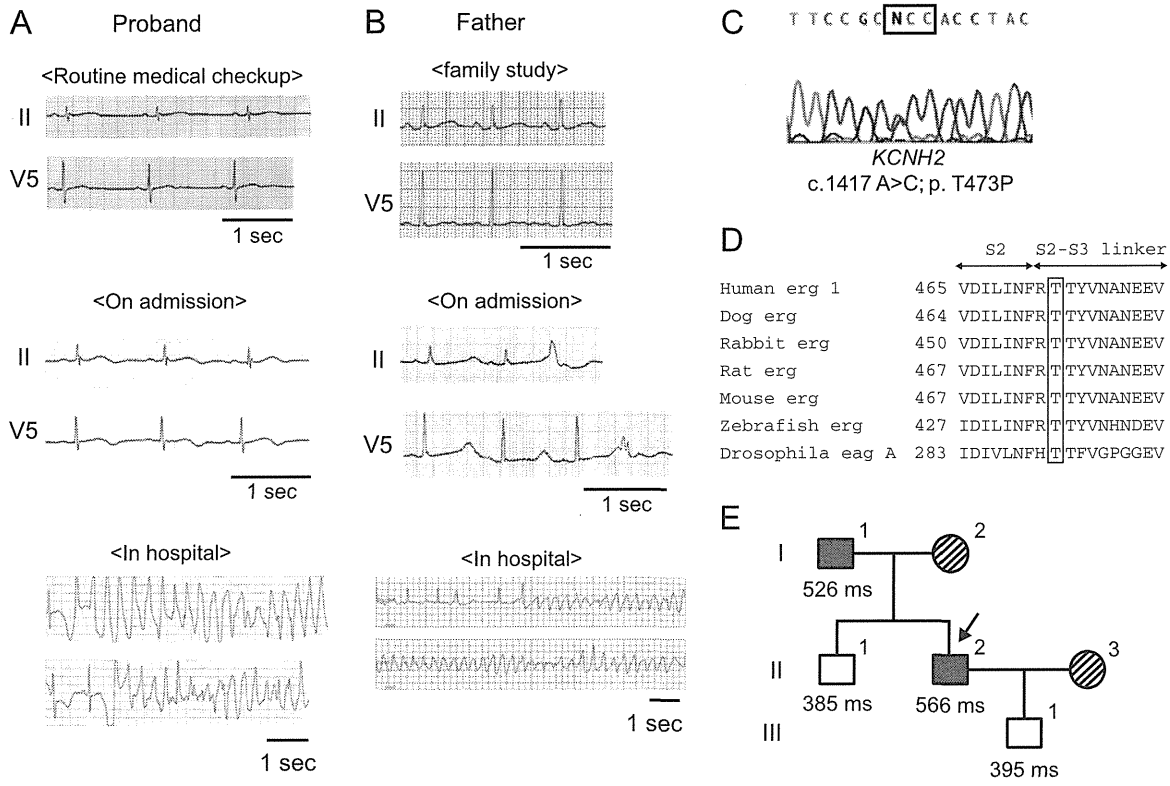

Figure 1 Electrocardiography and genetic analysis. **A:** Electrocardiograms (ECGs) of the proband. ECGs showed a mildly prolonged corrected QT (QTc) interval of 455 ms at a routine medical checkup and a significantly prolonged QTc interval of 566 ms upon hospital admission. Electrocardiographic tracing during the hospital stay showed torsades de pointes. **B:** ECGs of the proband's father. ECGs showed a prolonged QTc interval of 526 ms during a family study and a significantly prolonged QTc interval of 668 ms upon hospital admission. Electrocardiographic tracing during the hospital stay showed torsades de pointes. **C:** DNA sequence analysis of the *KCNH2* gene in the proband. A single nucleotide transition from A to C at nucleotide position 1417 in the *KCNH2* gene occurred in 2 affected family members. **D:** Amino acid sequences of the S2 and S2-S3 linkers of the hERG channel and 6 potassium channels. The box indicates the site of the T473P substitution. **E:** The pedigree and QTc intervals. The arrow in the pedigree indicates the proband. Numbers indicate the length of the QTc interval (in ms). Closed squares indicate heterozygous male patients with the *KCNH2* T473P mutation. Open squares indicate unaffected male patients without the *KCNH2* T473P mutation.

substitution at nucleotide 1417 of the *KCNH2* gene, resulting in an amino acid substitution from a highly conserved threonine to proline at position 473 of the Kv11.1 channel (Figures 1C–1E). This mutation is located in the transmembrane nonpore region and was not found in patients with the normal QTc interval or in the 150 healthy controls.

The proband's brother and son did not have a history of syncope and showed normal QTc interval in their ECGs (Figure 1E). Genetic analysis revealed that they did not have the T473P mutation.

Electrophysiological characteristics

To define the functional change of the T473P missense mutation, we transiently expressed hERG WT, hERG T473P, and hERG WT+hERG T473P in cultured mammalian cells for whole-cell voltage clamp measurements. Voltage clamp recording from WT showed a slowly activating outward current by step depolarizations (Figure 2A, left). By contrast, T473P did not express any functional channels (Figure 2A, center). When WT and T473P were coexpressed in CHO-K1 cells, the currents were less than one-fourth of control currents that were expected from expression of WT alone (Figure 2A, right). The current-voltage relationships for activating peak currents (Figure 2B) and tail currents (Figure 2C) were recorded during depolarizing pulses. The mean amplitude of the tail currents measured at −50 mV, after a depolarizing test pulse of +40 mV, was 10.5 ± 2.4 pA/pF for the WT+T473P channels (n = 20), which was significantly smaller than for WT-alone channels (40.5 ± 6.1 pA/pF; n = 15; $P < .05$). The T473P mutant did not generate any currents (n = 11). These results suggest that hERG T473P channels have dominant negative effects.

The amplitudes of the activating currents produced by the WT+T473P channels were too small to evaluate with the pulse protocol shown in Figure 2A. For this reason, we monitored recovery from inactivation (Figure 2D). The current density of the tail currents was −43.7 ± 10.5 pA/pF for WT+T473P (n = 15), which was significantly smaller than for WT alone (−105.5 ± 17.0 pA/pF; n = 15; $P < .05$) (Figure 2E). The normalized current-voltage relationships for tail currents of WT and WT+T473P showed that their mean $V_{1/2}$ values were −12.3 ± 0.9 mV (n = 15; slope factor 8.3 ± 0.5) and −10.9 ± 0.4 mV (n = 15; slope factor 11.0 ± 0.3), respectively (Figure 2F).

We next evaluated deactivation and steady-state inactivation of the T473P mutant channels. The fast and slow deactivation time constants showed no difference between

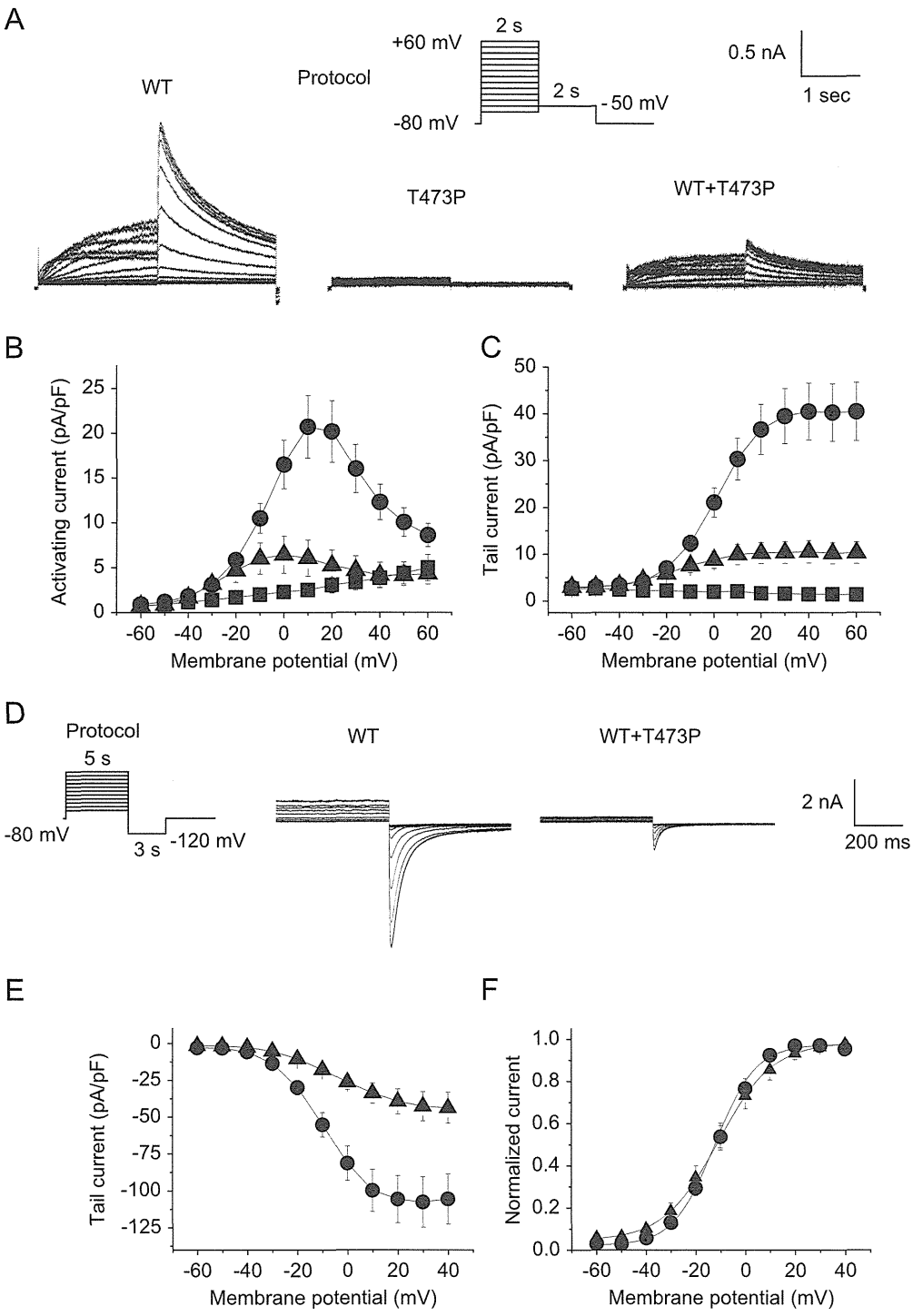

Figure 2 Functional characterization of hERG T473P in CHO-K1 cells. **A:** Representative generated currents in CHO-K1 cells, transfected with 1 μg of wild-type (WT) hERG alone (left), 1 μg of hERG T473P alone (middle), or 1 μg each of hERG WT and hERG T473P (right). Depolarizing pulses were applied from a holding potential of −80 mV to various potentials between −60 and +60 mV in 10 mV increments for 2 seconds, followed by a hyperpolarizing pulse to −50 mV for 2 seconds. **B and C:** I-V relationships for peak currents (B) and tail currents (C) in CHO-K1 cells transfected with WT alone (closed circle; n = 15), T473P (closed square; n = 11), or WT+T473P (closed triangle; n = 20). **D:** Representative generated currents in CHO-K1 cells transfected with 1 μg of WT alone or 1 μg each of WT and T473P. Currents were elicited by 5-second depolarizing pulses ranging from −60 to +40 mV, and peak tail currents were measured during a 3-second pulse to −120 mV and plotted as a function of the prepulse potential, with a holding potential of −80 mV. **E:** I-V relationships of tail currents for WT alone (closed circle; n = 15) and WT+T473P (closed triangle; n = 15). **F:** Mean amplitudes of normalized tail currents for WT alone (closed circle, n = 15) and WT+T473P (closed triangle, n = 15).

WT (n = 24) and WT+T473P channels (n = 15) (Figure 3A). Similarly, when the inactivation process was analyzed by using the voltage clamp method, the $V_{1/2}$ of inactivation yielded −56.9 ± 4.5 mV for WT (n = 20; slope factor 25.2 ± 3.3) and −59.9 ± 2.9 mV for WT+T473P (n = 20; slope factor 25.9 ± 2.1) (Figure 3B). Thus, no significant difference in the steady-state inactivation kinetics was observed as compared to WT.

Western blot analysis

To determine the effects of the T473P mutant on intracellular processing and trafficking, we assessed the glycosylation pattern by using Western blot analysis. As shown in Figure 4, WT resulted in 2 protein bands: a core-glycosylated form of about 135 kDa and a mature, fully glycosylated form of about 155 kDa. By contrast, the T473P mutant showed only 1 band of 135 kDa. This finding indicated that the T473P protein is incompletely processed and does not traffic correctly.

Effect of E4031 or thapsigargin on KCNH2 T473P mutation

Previous reports have shown that drugs that bind to hERG, such as E4031 and the SERCA inhibitor thapsigargin, can

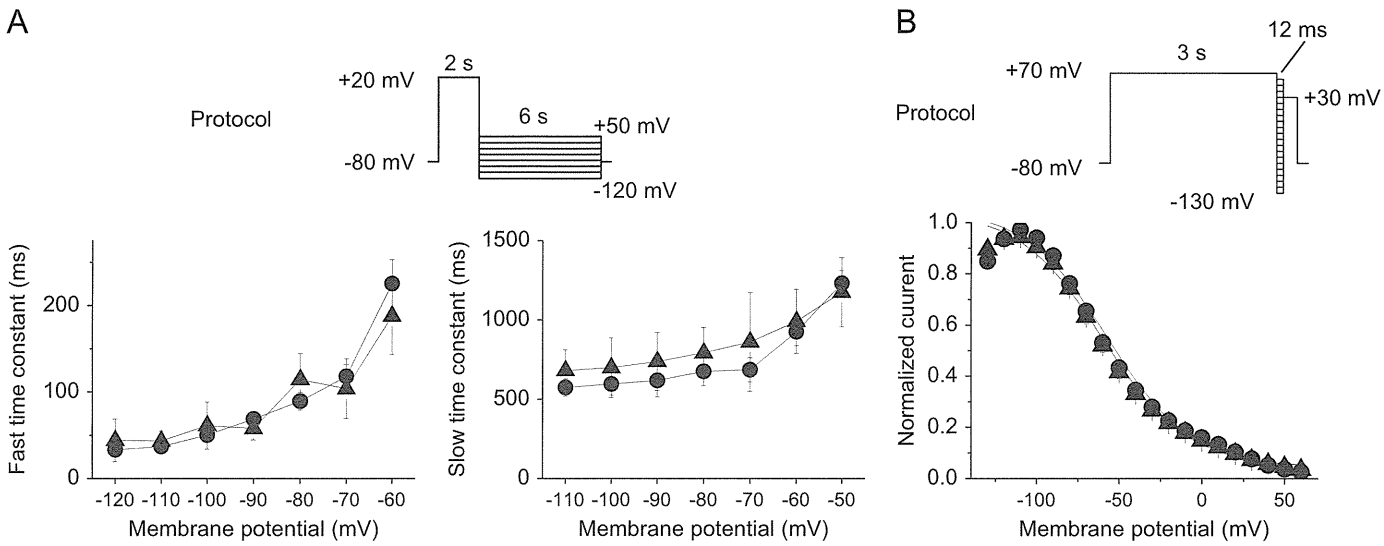

Figure 3 Deactivation and steady-state inactivation of hERG T473P in CHO-K1 cells. **A:** Deactivation time constants of wild-type (WT) (closed circle; n = 24) and WT+T473P (closed triangle; n = 15). Current was activated by 2-second pulses to +20 mV, followed by a return to test potentials between −50 and −100 mV. **B:** Normalized steady-state inactivation curves of WT (closed circle; n = 20) and WT+T473P (closed triangle; n = 20). To construct the inactivation curve, a voltage protocol (inset) was employed: a 3-second depolarizing pulse to inactivate hERG channels, followed by varying repolarizing pulses to a potential between −130 and +60 mV for 12 ms, and then a test pulse to +30 mV. The current amplitude at the test potential was normalized and plotted against the prepulse potential. Curves represent best fits to a Boltzmann function.

rescue trafficking defects of certain trafficking-deficient hERG variants[13–15]; therefore, we assessed the effects of the 2 drugs on T473P mutants. As a control, we included the hERG variant G601S, which is known to be rescued by this treatment, in our analysis. In cells expressing the trafficking-defective hERG G601S channels, the absolute peak tail current density in control condition was 19.2 ± 5.0 pA/pF (n = 17; Figure 5, left). After 24 hours of incubation with 10 μM E4031 or 1 μM thapsigargin, the current was significantly increased with an absolute peak tail current density of 58.0 ± 15.5 pA/pF (n = 10; $P < .05$) and 47.2 ± 14.6 pA/pF (n = 8; $P < .05$), respectively (Figure 5, left). Unlike the G601S-transfected cells, there was no current in cells expressing the hERG T473P channels in control condition (n = 9) (Figure 5, center). Administration of 10 μM E4031 or 1 μM thapsigargin for 24 hours resulted in no pharmacological rescue of hERG current (n = 9 and n = 8, respectively; Figure 5, center). We next studied the effect of E4031 or thapsigargin treatment on the coassembly of hERG WT and the T473P mutant (Figure 5, right). E4031 exposure significantly increased the absolute tail current density from 33.8 ± 5.7 pA/pF (n = 25) in control cells to 67.3 ± 16.0 pA/pF (n = 15; $P < .05$) in treated cells (Figure 5, right). By contrast, thapsigargin exposure did not affect *KCNH2* WT current; the absolute peak tail current density was 32.2 ± 6.9 pA/pF (n = 19) in treated cells, which was not significantly different from that in controls (Figure 5, right).

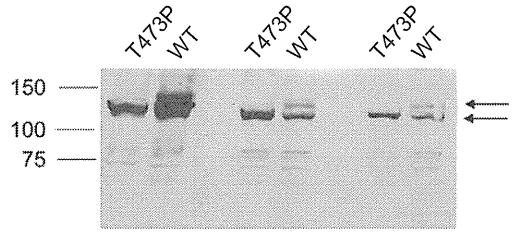

Figure 4 Incomplete glycosylation of hERG T473P indicates lack of intracellular processing and trafficking. In 3 independent experiments, hERG wild-type (WT) and hERG T473P were transfected into 100-mm dishes of CHO cells, as described previously. Two days posttransfection, whole-cell lysates were prepared as described previously by using a lysis buffer containing 50 mM Tris, 150 mM NaCl, 0.25% Triton X-100, and 5 mM NaF. Ten micrograms of cell extracts was loaded into a 7% polyacrylamide gel and prepared for polyacrylamide gel electrophoresis and Western blot analysis. Following transfer onto nitrocellulose membranes, rabbit anti-HERG 1 primary antibody (Alomone, 1:400) and HRP-linked donkey anti-rabbit secondary antibody (1:10,000, Amersham Biosciences/GE Healthcare Life Sciences) were applied. The blot was developed with ECL (Amersham Biosciences/GE Healthcare Life Sciences). Molecular weight markers are indicated on the left. The arrows on the right mark the position of the fully (top) and incompletely (bottom) glycosylated hERG proteins. In all 3 independent experiments, T473P remained incompletely glycosylated while hERG WT showed the mature glycosylation pattern.

Discussion

In this report, we describe a novel missense *KCNH2* mutation in patients who exhibited the congenital or acquired form of LQTS. The proband (Figure 1E, II-2 and arrow) was first diagnosed with epilepsy when he was 7 years old but continued to have repeated syncope in spite of continued antiepileptic medication. Previous reports indicate that patients are sometimes initially misdiagnosed with epilepsy and later receive a delayed diagnosis of LQTS.[16,17] The misdiagnosis of epilepsy and the treatment with antiepileptic drug medications is especially common in patients with LQT2.[17] We consider it likely that the index patient's repeated syncope was caused by TdP associated with LQTS, rather than epilepsy because 3 decades later he developed ventricular fibrillation and was diagnosed with LQTS. This is further supported by the fact that he did not experience

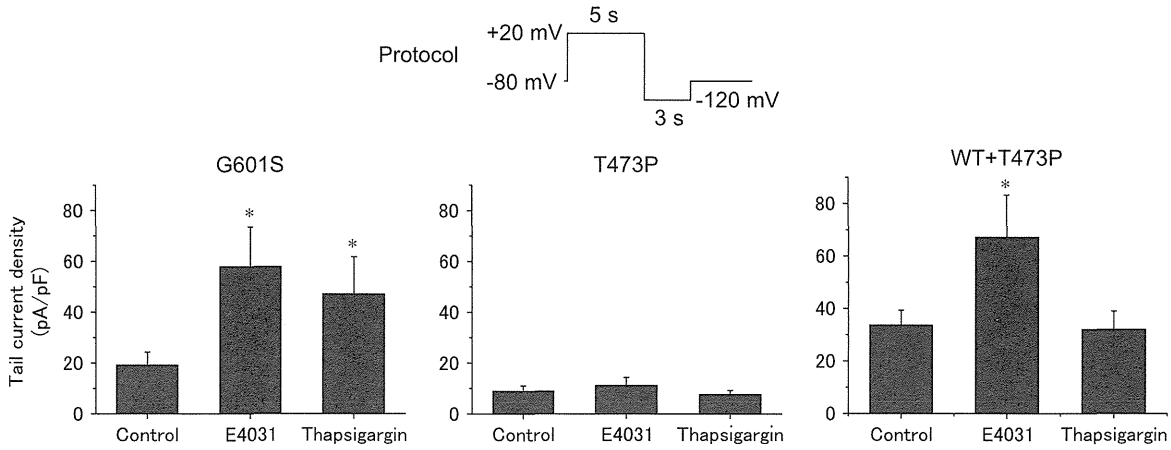

Figure 5 Effect of E4031 or thapsigargin on the trafficking-defective *KCNH2* mutations. The voltage clamp protocol is shown in the inset. From a holding potential of −80 mV, 5-second depolarizing pulses of +20 mV were applied, followed by a 3-second pulse of −120 mV. Absolute peak tail current densities of the G601S current, the T473P current, or the coexpressed WT+T473P current recorded at −120 mV from control cells, cells incubated in 10 μM of E4031 for 24 hours, or cells incubated in 1 μM of thapsigargin for 24 hours. $^{*}P < .05$ vs control cells.

syncope after the initiation of beta-blocker therapy. The proband's ECGs showed diurnal variability in the QTc interval, which might have resulted in his delayed diagnosis of LQTS; the QTc interval taken during daytime 1 month before the serious arrhythmic event was not significantly prolonged. According to previous reports, QTc intervals are longer at night than during the day in normal subjects.[18] The QTc interval and variability peak shortly after awakening, which may reflect increased autonomic instability and explain the increased vulnerability to ventricular tachycardia and sudden cardiac death in the morning.[18] Diurnal variability in QTc interval duration in LQTS has also been shown. Patients with LQT1 and LQT2 show trends for modest QTc shortening and lengthening, respectively, during the night compared with daytime, while patients with LQT3 show clear lengthening of the QTc interval during the night.[19] Goldenberg et al[20] reported that there was considerable variability in QTc measures in serial follow-up ECGs, and the maximum QTc interval provided incremental prognostic information in LQTS. Forty-one percent of the study patients had a maximum QTc of >500 ms, whereas only 25% of the patients had a baseline QTc interval of >500 ms during adolescence.[20]

The proband's father showed prolonged QTc interval and developed repeated TdP under hypokalemic conditions and after the administration of garenoxacin. Generally, the QT interval is prolonged by low extracellular potassium, which decreases I_{Kr} by enhancing I_{Kr} inactivation,[21] accelerating internalization and degradation of hERG channels,[22] and enhancing blockage of the hERG channels by extracellular sodium.[23] Some fluoroquinolones inhibit I_{Kr} and have been associated with TdP, resulting in QTc interval prolongation.[24] Garenoxacin, a novel quinolone antibiotic agent, is reportedly safe in healthy subjects.[25] However, in a separate report, TdP was induced by adding oral garenoxacin to disopyramide under hypokalemic conditions.[26] In this particular case, it was possible that reduced repolarization reserves due to enhanced I_{Kr} inhibition caused by a combination of *KCNH2* mutation, hypokalemia and oral garenoxacin contributed to QT interval prolongation and arrhythmia development.[27]

We identified a novel missense mutation in the transmembrane nonpore region of the hERG protein from patients with LQTS. Most mutations involving the pore region of *KCNH2* are missense mutations with dominant negative effects, whereas those in the nonpore regions are mostly associated with coassembly or trafficking abnormalities resulting in haplotype insufficiency.[28] A previous report showed that patients with missense mutations in the transmembrane nonpore region did not have significantly higher rates of cardiac events as compared to patients with missense mutations in the transmembrane pore region.[9] The *KCNH2* T473P mutation identified in this study showed trafficking abnormality and generated no current at all while exhibiting dominant negative effects on WT channels. Patients harboring this mutation showed a severe clinical course. The finding of a nonpore mutation that can cause a dominant negative effect is not novel: mutations in the *KCNH2*C-terminal region, A915fs+47X and G816V, also caused a trafficking defect that acted in a partially dominant negative manner.[29,30] In addition, previous studies reported several mutations that are located adjacent to position 473 of the *KCNH2* gene.[15,31–33] Interestingly, *KCNH2* D456Y,[15] F463L,[31] N470D,[15,32] and T474I[15,33] mutants all displayed protein trafficking deficiencies and caused a dominant negative effect on the WT hERG current. To explain this, a previous study proposed that the misfolded mutant subunits assemble with WT subunits in the endoplasmic reticulum to cause endoplasmic reticulum retention of the coassembled channels by the quality control system.[34]

Many trafficking-deficient LQT2 channels can be pharmacologically rescued by the administration of the drug E4031, which causes high-affinity inhibition of hERG channels, or the sarcoplasmic/endoplasmic reticulum Ca^{2+}-ATPase inhibitor thapsigargin.[13–15] In the electrophysiological study, homomeric T473P channels were not pharmacologically rescued by

either E4031 or thapsigargin (Figure 5, center). Consistent with these findings, our preliminary study showed that despite a 6-hour treatment with 1 μM thapsigargin, complete glycosylation of hERG T473P was still not observed on Western blot. However, our electrophysiological study showed that heteromeric channels (coassembled hERG WT and T473P subunits) were rescued only by E4031 (Figure 5, right). Thus, this indicated that T473P is partially and selectively rescued by E4031. A previous study showed that E4031 was also able to pharmacologically rescue the mutations adjacent to position 473 both upstream (N470D) and downstream (T474I), although thapsigargin could not.[15] This region may include trafficking-deficient mutations that can be rescued by E4031, but not by thapsigargin.

Our study identified a novel genetic change in the *KCNH2* gene, which indicated that certain mutations in the transmembrane nonpore region can result in protein trafficking defects and exhibit dominant negative effects. These mutations seem to be concentrated in the region between S2 and S2-S3 linkers of the hERG channel and may cause severe clinical course in affected patients.

References

1. Moss AJ, Schwartz PJ, Crampton RS, et al. The long QT syndrome: prospective longitudinal study of 328 families. Circulation 1991;84:1136–1144.
2. Napolitano C, Bloise R, Monteforte N, Priori SG. Sudden cardiac death and genetic ion channelopathies: long QT, Brugada, short QT, catecholaminergic polymorphic ventricular tachycardia, and idiopathic ventricular fibrillation. Circulation 2012;125:2027–2034.
3. Roden DM, Viswanathan PC. Genetics of acquired long QT syndrome. J Clin Invest 2005;115:2025–2032.
4. Splawski I, Shen J, Timothy KW, et al. Spectrum of mutations in long-QT syndrome genes: *KVLQT1*, *HERG*, *SCN5A*, *KCNE1*, and *KCNE2*. Circulation 2000;102:1178–1185.
5. Hayashi K, Shimizu M, Ino H, et al. Characterization of a novel missense mutation *E637K* in the pore-S6 loop of HERG in a patient with long QT syndrome. Cardiovasc Res 2002;54:67–76.
6. Hayashi K, Shimizu M, Ino H, et al. Probucol aggravates long QT syndrome associated with a novel missense mutation M124T in the N-terminus of HERG. Clin Sci (Lond) 2004;107:175–182.
7. Itoh H, Sakaguchi T, Ding WG, et al. Latent genetic backgrounds and molecular pathogenesis in drug-induced long-QT syndrome. Circ Arrhythm Electrophysiol 2009;2:511–523.
8. Moss AJ, Zareba W, Kaufman ES, et al. Increased risk of arrhythmic events in long-QT syndrome with mutations in the pore region of the human ether-a-go-go-related gene potassium channel. Circulation 2002;105:794–799.
9. Shimizu W, Moss AJ, Wilde AA, et al. Genotype-phenotype aspects of type 2 long QT syndrome. J Am Coll Cardiol 2009;54:2052–2062.
10. Hayashi K, Fujino N, Ino H, et al. A KCR1 variant implicated in susceptibility to the long QT syndrome. J Mol Cell Cardiol 2011;50:50–57.
11. Kupershmidt S, Yang IC, Hayashi K, et al. The IKr drug response is modulated by KCR1 in transfected cardiac and noncardiac cell lines. FASEB J 2003;17:2263–2265.
12. Nakajima T, Hayashi K, Viswanathan PC, et al. HERG is protected from pharmacological block by alpha-1,2-glucosyltransferase function. J Biol Chem 2007;282:5506–5513.
13. Zhou Z, Gong Q. January CT. Correction of defective protein trafficking of a mutant HERG potassium channel in human long QT syndrome: pharmacological and temperature effects. J Biol Chem 1999;274:31123–31126.
14. Delisle BP, Anderson CL, Balijepalli RC, et al. Thapsigargin selectively rescues the trafficking defective LQT2 channels G601S and F805C. J Biol Chem 2003;278:35749–35754.
15. Anderson CL, Delisle BP, Anson BD, et al. Most LQT2 mutations reduce Kv11.1 (hERG) current by a class 2 (trafficking-deficient) mechanism. Circulation 2006;113:365–373.
16. MacCormick JM, McAlister H, Crawford J, et al. Misdiagnosis of long QT syndrome as epilepsy at first presentation. Ann Emerg Med 2009;54:26–32.
17. Johnson JN, Hofman N, Haglund CM, et al. Identification of a possible pathogenic link between congenital long QT syndrome and epilepsy. Neurology 2009;72:224–231.
18. Molnar J, Zhang F, Weiss J, Ehlert FA, Rosenthal JE. Diurnal pattern of QTc interval: how long is prolonged? Possible relation to circadian triggers of cardiovascular events. J Am Coll Cardiol 1996;27:76–83.
19. Kaufman ES, Priori SG, Napolitano C, et al. Electrocardiographic prediction of abnormal genotype in congenital long QT syndrome: experience in 101 related family members. J Cardiovasc Electrophysiol 2001;12:455–461.
20. Goldenberg I, Mathew J, Moss AJ, et al. Corrected QT variability in serial electrocardiograms in long QT syndrome: the importance of the maximum corrected QT for risk stratification. J Am Coll Cardiol 2006;48:1047–1052.
21. Yang T, Snyders DJ, Roden DM. Rapid inactivation determines the rectification and $[K^+]_o$ dependence of the rapid component of the delayed rectifier K^+ current in cardiac cells. Circ Res 1997;80:782–789.
22. Guo J, Massaeli H, Xu J, et al. Extracellular K^+ concentration controls cell surface density of IKr in rabbit hearts and of the HERG channel in human cell lines. J Clin Invest 2009;119:2745–2757.
23. Numaguchi H, Johnson JP, Jr, Petersen CI, Balser JR. A sensitive mechanism for cation modulation of potassium current. Nat Neurosci 2000;3:429–430.
24. Kang J, Wang L, Chen XL, Triggle DJ, Rampe D. Interactions of a series of fluoroquinolone antibacterial drugs with the human cardiac K^+ channel HERG. Mol Pharmacol 2001;59:122–126.
25. Wang Z, Grasela DM, Krishna G. Retrospective analysis of electrocardiographic changes after administration of oral or intravenous garenoxacin in five phase I, placebo-controlled studies in healthy volunteers. Clin Ther 2007;29:1098–1106.
26. Miyamoto K, Kawai H, Aoyama R, et al. Torsades de pointes induced by a combination of garenoxacin and disopyramide and other cytochrome P450, family 3, subfamily A polypeptide-4-influencing drugs during hypokalemia due to licorice. Clin Exp Nephrol 2010;14:164–167.
27. Roden DM, Long QT. syndrome: reduced repolarization reserve and the genetic link. J Intern Med 2006;259:59–69.
28. January CT, Gong Q, Zhou Z. Long QT syndrome: cellular basis and arrhythmia mechanism in LQT2. J Cardiovasc Electrophysiol 2000;11:1413–1418.
29. Christe G, Theriault O, Chahine M, et al. A new C-terminal hERG mutation A915fs+47X associated with symptomatic LQT2 and auditory-trigger syncope. Heart Rhythm 2008;5:1577–1586.
30. Krishnan Y, Zheng R, Walsh C, Tang Y, McDonald TV. Partially dominant mutant channel defect corresponding with intermediate LQT2 phenotype. Pacing Clin Electrophysiol 2012;35:3–16.
31. Yang HT, Sun CF, Cui CC, et al. HERG-F463L potassium channels linked to long QT syndrome reduce I(Kr) current by a trafficking-deficient mechanism. Clin Exp Pharmacol Physiol 2009;36:822–827.
32. Sanguinetti MC, Curran ME, Spector PS, Keating MT. Spectrum of HERG K^+-channel dysfunction in an inherited cardiac arrhythmia. Proc Natl Acad Sci U S A 1996;93:2208–2212.
33. Nakajima T, Furukawa T, Tanaka T, et al. Novel mechanism of HERG current suppression in LQT2: shift in voltage dependence of HERG inactivation. Circ Res 1998;83:415–422.
34. Gong Q, Anderson CL. January CT, Zhou Z. Pharmacological rescue of trafficking defective HERG channels formed by coassembly of wild-type and long QT mutant N470D subunits. Am J Physiol Heart Circ Physiol 2004;287:H652–H658.